Insulator-to-metal transition in $(R,\mathrm{Ca})\mathrm{VO}_3$

M. H. Sage, G. R. Blake, and T. T. M. Palstra*
Solid State Chemistry Laboratory, Zernike Institute for Advanced Materials, University of Groningen, Nijenborgh 4, 9747 AG Groningen, The Netherlands

(Received 19 July 2007; revised manuscript received 11 March 2008; published 18 April 2008)

We have carried out a comprehensive study of the transport and thermodynamic properties of $R_{1-x}\mathrm{Ca}_x\mathrm{VO}_3$ (R=Pr, Sm, and Y), obtaining detailed information on the nature of the insulator-metal transition induced by Ca doping. The behavior of the electronic term of the specific heat as a function of doping indicates that the transition is achieved by the use of band-filling control. We find that disorder plays an important role in the transition, which is manifested by weak localization effects in the vicinity of the critical doping level. The metallic state in all three materials is characterized by the presence of strong electron correlations.

DOI: 10.1103/PhysRevB.77.155121 PACS number(s): 65.40.Ba, 71.30.+h, 72.15.Rn, 72.80.Ga

INTRODUCTION

The insulator-metal (IM) transition in transition metal oxides has been widely studied.[1] One way to obtain a metallic state from a Mott insulator is to reduce electron correlation effects by the application of external pressure or by chemical substitution with isovalent ions of different radii. This has the effect of tuning the one-electron bandwidth at a constant level of band filling. Alternatively, an IM transition can be induced by controlling the filling of the band through chemical doping with ions of different valences or by introducing nonstoichiometry. $R\mathrm{VO}_3$ compounds are defined as Mott insulators in the broad sense of the definition and more precisely as Mott–Hubbard insulators in the Zaanen–Sawatzky–Allen classification scheme.[2] The IM transition can easily be achieved by band-filling control through the substitution of trivalent rare-earth cations for divalent cations such as Ca^{2+} and Sr^{2+}, changing an equivalent number of V^{3+} to V^{4+}.

The IM transition induced by band-filling control in $R\mathrm{VO}_3$ has been investigated since the 1970s. The most widely studied system is $\mathrm{La}_{1-x}\mathrm{Sr}_x\mathrm{VO}_3$, in which the IM transition takes place at a critical doping level reported to be between x_c=0.18 and x_c=0.23.[3–10] This appears to be a good example of an Anderson transition, with a region of variable-range hopping conduction being present immediately above x_c. The variable-range hopping arises from the localization of electrons due to factors including cation disorder between La and Sr. Above x_c, the antiferromagnetic ordering observed in the low-doped insulating (AFI) phase persists in the ground state over a considerable range of x, while the carrier density gradually increases.[7,8] Eventually, a transition to a paramagnetic metallic (PM) phase takes place. The nature of both the intermediate, antiferromagnetic metallic (AFM) phase and the PM phase near the AFM-PM transition has been the subject of debate; significant deviation from Fermi-liquid behavior has been observed in both.[8] The resistivity in the metallic phase is strongly influenced by antiferromagnetic (AF) spin fluctuations. We note that $\mathrm{La}_{1-x}\mathrm{Sr}_x\mathrm{VO}_3$ appears to be unique among the doped $R\mathrm{VO}_3$ materials in that orbital ordering is retained at doping levels up to x_c, where a first-order structural phase transition takes place; the orbital ordering melts at doping levels well below x_c for all other doped $R\mathrm{VO}_3$ that have been investigated. Thus, the critical behavior in the vicinity of the IM transition for $\mathrm{La}_{1-x}\mathrm{Sr}_x\mathrm{VO}_3$ may be strongly influenced by orbital fluctuations and lattice dynamics.[8]

Two other doped $R\mathrm{VO}_3$ systems have received significant attention. The IM transition in $\mathrm{La}_{1-x}\mathrm{Ca}_x\mathrm{VO}_3$ takes place at a critical doping level close to x_c=0.2 and there are signs that it also undergoes an Anderson transition.[11–14] However, deviations from Fermi-liquid behavior are observed well beyond x_c and it appears that chemical inhomogeneity or electronic phase separation may be an inherent feature of this system.[12–14] In $\mathrm{Y}_{1-x}\mathrm{Ca}_x\mathrm{VO}_3$, the bandwidth is smaller since Y^{3+} has a smaller ionic radius than La^{3+} and the perovskite structure is more distorted; the V-O-V bond angles deviate more from linearity. The consequence is that a higher number of doped carriers are necessary to achieve the IM transition. However, there is little consensus on where the transition occurs, with reported doping levels varying between x_c =0.35 and x_c=0.65.[15–20] Cintolesi *et al.*[19] suggested that a fraction of the low-doped AFI phase remains in the sample up to high doping levels. This may help explain discrepancies in magnetization data between different studies.[20–22] Nevertheless, there appears to be a region of weak localization and variable-range hopping in the vicinity of the IM transition, similar to $\mathrm{La}_{1-x}\mathrm{Sr}_x\mathrm{VO}_3$.

There is a general lack of detailed, quantitative transport measurements in the literature on doped $R\mathrm{VO}_3$, leading to a lack of consensus on the nature of the doping-induced IM transition in these materials. For example, the Seebeck effect has been little studied, although it can provide important insight into the character of the transition. Furthermore, the transport properties measured in different studies are often in conflict with each other. There is thus a need for a systematic investigation of the transport properties of doped $R\mathrm{VO}_3$ as a function of both carrier concentration and perovskite tolerance factor (one-electron bandwidth). We have investigated the IM transition in Ca-doped PrVO_3, SmVO_3, and YVO_3, which represent compounds with large, medium, and small rare-earth cations. We observe that the transition is reached by band-filling control; disorder plays an important role, which is manifested by weak localization effects in all three series of materials. The metallic state is characterized by the presence of strong electron correlations.

 ©2008 The American Physical Society

I. EXPERIMENTAL RESULTS

Polycrystalline samples of $(R,\mathrm{Ca})VO_3$ were prepared by the chemical reduction of $(R,\mathrm{Ca})VO_4$ at 1400 °C under a H_2/N_2 atmosphere. The RVO_4 powders were prepared by solid state reaction, using predried R_2O_3 (99.9%), $CaCO_3$ (99.95%), and a 2% excess of V_2O_5 (99.95%) to compensate for the volatility of vanadium. X-ray diffraction measurements showed the samples to be pure. We attempted the growth of single crystals by using the traveling solvent floating zone method, but these materials melt incongruently and we were thus unable to obtain homogeneous crystals. The RVO_3 powder samples were pressed into bar-shaped pellets for the transport measurements; a four-wire setup was used and the experiments were performed using a Quantum Design Physical Properties Measurement System (PPMS). A home-made Seebeck platform incorporating a MMR Seebeck stage (MMR Technologies, Inc.) was connected to a standard sample puck in order to measure thermopower in the PPMS. Specific heat measurements at constant pressure were performed on pellets by using a relaxation method in the PPMS.

X-ray diffraction showed that all of the Ca-doped materials adopt the orthorhombic perovskite structure with space group *Pbnm*, as is the case for the undoped RVO_3 compounds at room temperature.[23–25] We found that the IM transition had little effect on the structural properties; details can be found elsewhere.[26] All three series of doped materials exhibit AF ordering that persists in the ground state beyond the critical doping level x_c for the IM transition. Thus, on increasing the level of doping, they all undergo an AFI to AFM transition before eventually becoming Pauli paramagnetic metals. Details of the magnetic properties can be found elsewhere,[26] while we focus on the transport and thermodynamic properties in the current report.

A. Resistivity

The measured resistivity as a function of temperature and doping is shown for all three series of compounds in Fig. 1. The temperature range over which the resistivity is low enough to measure increases with Ca doping, as the samples become more conducting. Fits of the resistivity curves showed that for low Ca doping ($x \leqslant 0.3$ for $Y_{1-x}Ca_xVO_3$ and $x \leqslant 0.2$ for the other two series), thermally activated behavior is present:

$$\rho = \rho_{01} \exp\left(\frac{E_a}{k_B T}\right). \tag{1}$$

In all cases, the extracted activation energy E_a decreases with doping (Tables I–III). In the case of $Y_{1-x}Ca_xVO_3$, our values are consistent with those reported by Kasuya *et al.*[16] and Cintolesi *et al.*,[19] but significantly smaller than the 0.2 eV reported by Nishihara *et al.*[17] for $Y_{0.7}Ca_{0.3}VO_3$. The activation energies of the other two systems are of similar magnitude to that of the Y series.

For $0.1 \leqslant x \leqslant 0.2$ in the Pr series and $0.2 \leqslant x \leqslant 0.3$ in the Y series, the resistivity below ~160 K does not follow an activated behavior and is instead characteristic of variable-range hopping:[27]

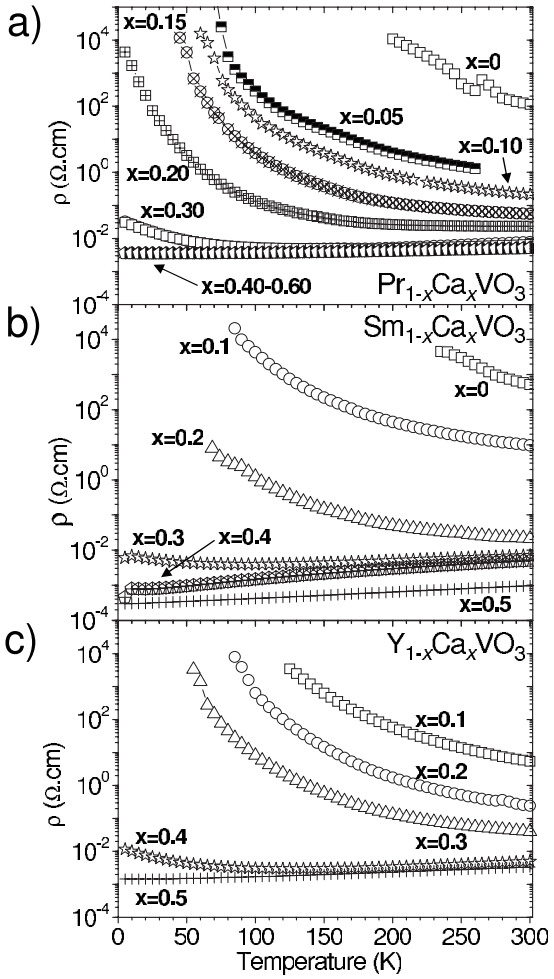

FIG. 1. Temperature dependence of the resistivity of (a) $Pr_{1-x}Ca_xVO_3$, (b) $Sm_{1-x}Ca_xVO_3$, and (c) $Y_{1-x}Ca_xVO_3$. Note that ρ is plotted on a logarithmic scale.

$$\rho = \rho_{02} \exp\left(\frac{T_0}{T}\right)^{1/4}. \tag{2}$$

T_0 is a parameter related to the density of localized states at the Fermi level $N(E_F)$ by the following equation:

$$T_0 = \frac{24\alpha^3}{\pi N(E_F) k_B}. \tag{3}$$

By using T_0 and a reasonable value for α of 0.2 $Å^{-1}$ (α^{-1} is the decay rate of the wave function associated with the charge carriers and is commonly of the order of ~5 Å in transition metal oxides, corresponding in our case to the approximate distance between next-nearest-neighbor V atoms),[28–31] $N(E_F)$ can be extracted. As expected, $N(E_F)$ rapidly increases with doping (Tables I and III).

Maiti *et al.*[13] reported that in $La_{1-x}Ca_xVO_3$, the temperature dependence of the resistivity can be fitted over the entire temperature range by using a combination of thermally activated behavior and variable-range hopping. However, in $Pr_{1-x}Ca_xVO_3$ and $Y_{1-x}Ca_xVO_3$, we find that each type independently contributes to the resistivity depending on the temperature range. Although none of our $Sm_{1-x}Ca_xVO_3$ samples

TABLE I. Parameters used to fit the temperature dependence of the resistivity in $Pr_{1-x}Ca_xVO_3$. E_a and ρ_{01} are the activation energy and prefactor for thermally activated behavior [Eq. (1)]. ρ_{02}, T_0, and $N(E_F)$ are the residual resistivity, the extracted temperature, and the density of localized states at the Fermi level for variable-range hopping [Eqs. (2) and (3)]. ρ_{03}, $a_{e\text{-}ph}$, and $a_{e\text{-}e}$ are the residual resistivity, the electron-phonon scattering, and the electron-electron interaction in the Fermi-liquid region [Eq. (4)]. σ_0 and β are the prefactor and $\sqrt{T}$ coefficient of the conductivity [Eq. (5)].

x	E_a (eV)	ρ_{01} (Ω cm)	ρ_{02} (Ω cm)	T_0 (K)	$N(E_F)$ (cm^{-3} eV^{-1})	ρ_{03} (Ω cm)	$a_{e\text{-}ph}$ (Ω cm K^{-1})	$a_{e\text{-}e}$ (Ω cm K^{-2})	σ_0 (Ω^{-1} cm^{-1})	β (Ω^{-1} cm^{-1} $\mathrm{K}^{-0.5}$)
0	0.179	0.36								
0.05	0.074	0.050								
0.10	0.066	0.020	4.9×10^{-14}	1.4×10^{8}	5.1×10^{18}					
0.15	0.059	0.0012	3.0×10^{-11}	3.8×10^{7}	1.8×10^{19}					
0.20	0.046	0.0006	9.5×10^{-9}	7.4×10^{6}	9.6×10^{19}					
0.25 ($T\geqslant130$ K)						0.0037	0	4.3×10^{-8}		
0.25 ($T\leqslant25$ K)									2.9	11
0.30 ($T\geqslant170$ K)						0.0037	0	3.1×10^{-8}		
0.30 ($T\leqslant15$ K)									4.8	11
0.40 ($T\geqslant80$ K)						0.0035	0	2.0×10^{-8}		
0.40 ($T\leqslant20$ K)									270	2.6
0.50 ($T\geqslant145$ K)						0.0038	0	2.1×10^{-8}		
0.50 (50 K$<T<$145 K)						0.0035	0	3.1×10^{-8}		
0.60 ($T\geqslant50$ K)						0.0035	0	1.8×10^{-8}		
0.60 ($T\leqslant15$ K)									280	2.1

display evidence of variable-range hopping, we cannot rule out its occurrence in a narrow doping range between $x=0.2$ and $x=0.3$.

As the Ca concentration increases further, the critical doping level is reached and an IM transition takes place. A metallic character is observed for samples with $x\geqslant0.25$ in $Pr_{1-x}Ca_xVO_3$, $x\geqslant0.3$ in $Sm_{1-x}Ca_xVO_3$, and $x\geqslant0.4$ in $Y_{1-x}Ca_xVO_3$. Above x_c, the resistivity can be fitted over the majority of the temperature range by the following equation:

$$\rho=\rho_{03}+a_{e\text{-}ph}T+a_{e\text{-}e}T^2, \tag{4}$$

where ρ_{03} is the residual resistivity, $a_{e\text{-}ph}$ is a measure of the electron-phonon scattering, and $a_{e\text{-}e}$ quantifies the electron-electron interactions for a strongly correlated Fermi liquid. The fitted parameters and relevant temperature ranges are summarized in Tables I–III. A deviation from Fermi-liquid behavior is apparent at low temperature for the $Pr_{1-x}Ca_xVO_3$ ($x\geqslant0.25$), $Sm_{0.7}Ca_{0.3}VO_3$, and $Y_{0.6}Ca_{0.4}VO_3$ samples, where an upturn in the resistivity occurs. In this range, the conductivity follows a temperature dependence of the form

$$\sigma=\sigma_0+\beta\sqrt{T}, \tag{5}$$

where σ_0 is the finite conductivity at zero temperature. A similar upturn in resistivity has previously been observed in the metallic phases of $La_{1-x}Sr_xVO_3$,[7] $La_{1-x}Ca_xVO_3$,[13] and

TABLE II. Parameters used to fit the temperature dependence of the resistivity in $Sm_{1-x}Ca_xVO_3$. E_a and ρ_{01} are the activation energy and prefactor for thermally activated behavior [Eq. (1)]. ρ_{03}, $a_{e\text{-}ph}$, and $a_{e\text{-}e}$ are the residual resistivity, the electron-phonon scattering, and the electron-electron interaction in the Fermi-liquid region [Eq. (4)]. σ_0 and β are the prefactor and $\sqrt{T}$ coefficient of the conductivity [Eq. (5)].

x	E_a (eV)	ρ_{01} (Ω cm)	ρ_{03} (Ω cm)	$a_{e\text{-}ph}$ (Ω cm K^{-1})	$a_{e\text{-}e}$ (Ω cm K^{-2})	σ_0 (Ω^{-1} cm^{-1})	β (Ω^{-1} cm^{-1} $\mathrm{K}^{-0.5}$)
0	0.232	0.061					
0.1	0.088	0.030					
0.2	0.054	0.0024					
0.3 ($T\geqslant135$ K)			0.0033	0	4.1×10^{-8}		
0.3 ($T\leqslant60$ K)						79	21
0.4 ($T\geqslant40$ K)			0.00054	6.4×10^{-6}	2.8×10^{-8}		
0.4 ($T\leqslant35$ K)			0.00076	0	6.0×10^{-8}		
0.5			0.00029	7.1×10^{-7}	5.1×10^{-9}		

TABLE III. Parameters used to fit the temperature dependence of the resistivity in $Y_{1-x}Ca_xVO_3$. E_a and ρ_{01} are the activation energy and prefactor for thermally activated behavior [Eq. (1)]. ρ_{02}, T_0, and $N(E_F)$ are the residual resistivity, the extracted temperature, and the density of localized states at the Fermi level for variable-range hopping [Eqs. (2) and (3)]. ρ_{03}, $a_{e\text{-}ph}$, and $a_{e\text{-}e}$ are the residual resistivity, the electron-phonon scattering, and the electron-electron interaction in the Fermi-liquid region [Eq. (4)]. σ_0 and β are the prefactor and $\sqrt{T}$ coefficient of the conductivity [Eq. (5)].

x	E_a (eV)	ρ_{01} (Ω cm)	ρ_{02} (Ω cm)	T_0 (K)	$N(E_F)$ (cm^{-3} eV^{-1})	ρ_{03} (Ω cm)	$a_{e\text{-}ph}$ (Ω cm K^{-1})	$a_{e\text{-}e}$ (Ω cm K^{-2})	σ_0 (Ω^{-1} cm^{-1})	β (Ω^{-1} cm^{-1} $K^{-0.5}$)
0.1	0.124	0.045								
0.2	0.106	0.0038	1.6×10^{-14}	2.1×10^{8}	3.4×10^{18}					
0.3	0.064	0.0032	7.5×10^{-12}	5.9×10^{7}	1.2×10^{19}					
0.4 ($T\geqslant170$ K)						0.0021	0	3.1×10^{-8}		
0.4 ($T\leqslant40$ K)									8.0	29
0.5						0.0014	1.0×10^{-6}	1.8×10^{-8}		

$Y_{1-x}Ca_xVO_3$ (Ref. 17) in the vicinity of the IM transition; its origin will be discussed below. In an intermediate temperature region, the resistivity can be fitted well by using a combination of a linear T dependence, showing the significance of electron-phonon interactions in this temperature interval, and a $T^{-0.5}$ dependence.

For higher Ca concentrations, the resistivity of the Sm and Y series exhibits a Fermi-liquid behavior according to Eq. (4) over the entire temperature range, with the T^2 electron-electron interaction term dominating. This is in agreement with the resistivity measurements of Nishihara *et al.*[17] on $Y_{1-x}Ca_xVO_3$, but in contrast to the purely linear dependence of resistivity reported by Cintolesi *et al.*[19] on the same system. For the Pr series, the low-temperature upturn is still visible for the $x=0.6$ sample, which is the highest doped sample that we investigated.

The resistivity is presented as a function of rare-earth radius for $x=0$, $x=0.1$, and $x=0.3$ in Fig. 2 in order to illustrate the systematic bandwidth dependence. As expected, the resistivity at a given doping level generally increases with decreasing bandwidth.

B. Seebeck effect

The results of the Seebeck measurements are presented in Fig. 3. At doping levels well below x_c, the Seebeck coefficient typically exhibits a thermally activated behavior and can be fitted as follows:

$$S = \frac{k_B}{e}\frac{E_a}{k_B T}, \tag{6}$$

where e is the elementary unit of charge. The extracted activation energies are all much smaller than those obtained from the resistivity measurements, indicating a small-polaron conduction of the mobile charge carriers.[12] At low temperatures, the mobile charge carriers are frozen out. Some additional features are noticeable; for example, in $Y_{0.8}Ca_{0.2}VO_3$, the behavior of the thermopower below 160 K is characteristic of phonon drag arising from the dominant electron-phonon scattering. This is in agreement with the resistivity measurements, which showed that electron-phonon interactions are strongest in this temperature region.

As x_c is approached from the insulating side of the transition, the thermopower markedly decreases and can no longer be described by Eq. (6) in the temperature range of the measurements. Despite the resistivity still being characteristic of a semiconductor, the thermopower of samples in all three series becomes smaller than $k_B/e=87$ μV/K, which

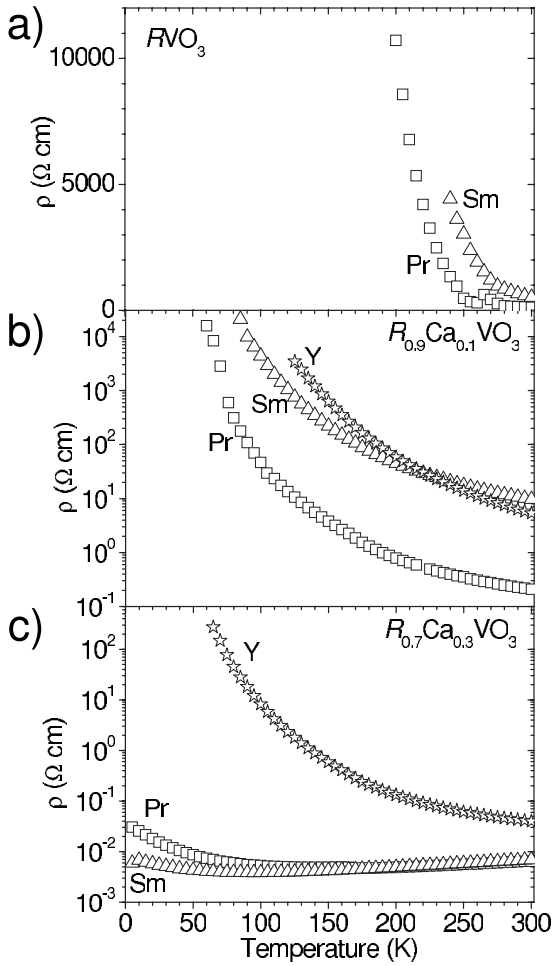

FIG. 2. Temperature dependence of the resistivity of $R_{1-x}Ca_xVO_3$ for (a) $x=0$, (b) $x=0.1$, and (c) $x=0.3$. Note that ρ is plotted on a logarithmic scale.

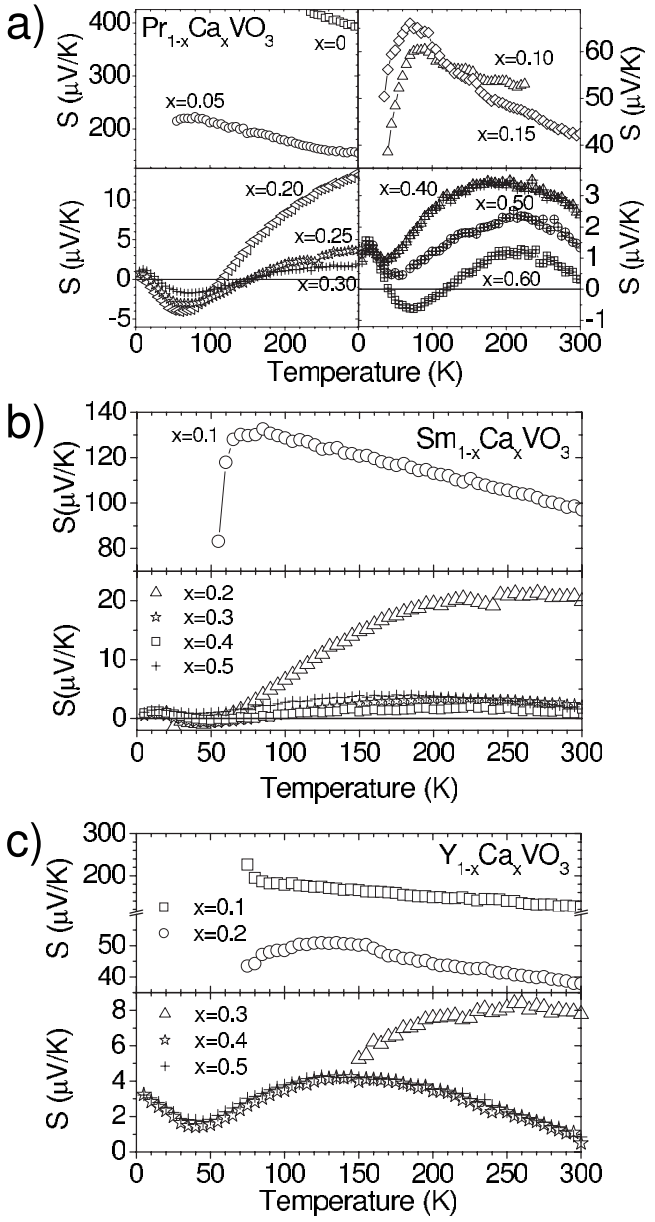

FIG. 3. Temperature dependence of the Seebeck coefficient in (a) $Pr_{1-x}Ca_xVO_3$, (b) $Sm_{1-x}Ca_xVO_3$, and (c) $Y_{1-x}Ca_xVO_3$.

is the value at which samples can be considered metallic.

In the metallic doping region at $x \geqslant x_c$, it is expected that the thermopower should obey the following temperature dependence:

$$S = \frac{k_B}{e}\frac{k_B T}{E_F}. \tag{7}$$

However, our samples show a substantial deviation from Fermi-liquid behavior, generally displaying a broad maximum between 150 and 200 K, then falling with temperature to reach a minimum at ~50 K and increasing again at low temperature. This trend is most pronounced for samples in the Pr series, but also takes place to a lesser extent in the other two series. For some samples in the Pr and Sm series, the Seebeck coefficient twice changes sign from positive to negative in the vicinity of the minimum. This anomalous behavior is continued to doping levels well beyond x_c in all three series, and a similar temperature dependence has previously been observed over a wide doping range in $La_{1-x}Ca_xVO_3$.[12] The temperature dependence of the thermopower is strongly affected by factors such as electron-phonon scattering and electron-electron correlation and localization. It appears that in our systems, several competing physical mechanisms are present at the same time.

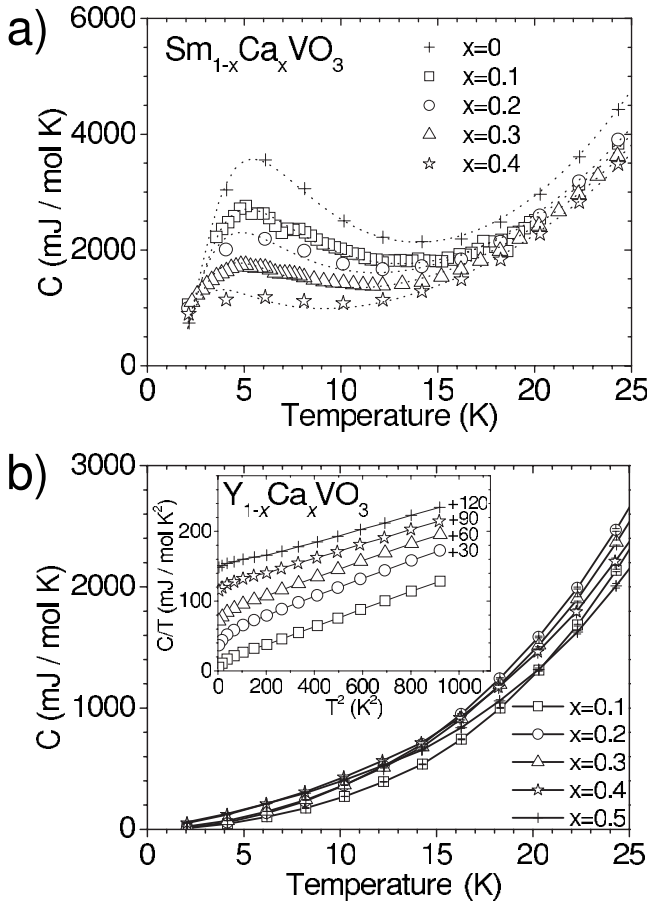

FIG. 4. Evolution of the low-temperature specific heat of (a) $Sm_{1-x}Ca_xVO_3$ and (b) $Y_{1-x}Ca_xVO_3$. The dotted lines in (a) are fits to the Schottky anomaly by using Eq. (8). The inset of (b) shows plots of C/T versus T^2, in which, for reasons of clarity, the data for $x \geqslant 0.2$ have been offset by the factors indicated.

C. Specific heat

The temperature dependence of the specific heat, measured for samples in the Sm and Y series, is plotted in Fig. 4. For $Y_{1-x}Ca_xVO_3$, a plot of C/T versus T^2 is shown in the inset. We performed fits of the linear portion of these curves in order to extract the electronic term γ and the lattice term β. In $Sm_{1-x}Ca_xVO_3$, a Schottky-type anomaly is apparent below ~20 K, which probably originates from the crystal field splitting of Sm^{3+}. Schottky anomalies have previously been observed in other Sm-containing compounds,[32] and we used the following equation at low temperature to fit the specific heat curve:

TABLE IV. Fitted parameters for Schottky anomaly in $Sm_{1-x}Ca_xVO_3$ as a function of doping.

x	n	Δ (K)	γ (mJ mol^{-1} K^{-2})	β (mJ mol^{-1} K^{-3})
0	0.97(1)	13.1(1)	0	0.64(1)
0.1	0.70(1)	12.1(2)	24(4)	0.58(1)
0.2	0.58(3)	11.1(5)	37(10)	0.57(2)
0.3	0.43(1)	10.6(2)	43(4)	0.55(1)
0.4	0.32(2)	8.7(5)	42(6)	0.55(1)

$$C(T) = nR\left(\frac{\Delta}{T}\right)^2 \frac{\exp(\Delta/T)}{[1+\exp(\Delta/T)]^2} + \gamma T + \beta T^3. \qquad (8)$$

The first part of this equation is the Schottky contribution to the specific heat, corresponding to a two-level Schottky function, where n is the fraction of magnetic Sm, R is the universal gas constant, and Δ is the Kramers doublet splitting. The parameters extracted from our fit are summarized in Table IV. It is apparent that Δ and n decrease with doping, suggesting that the proportion of Sm^{3+} decreases.

We plot the electronic term γ as a function of doping for $Sm_{1-x}Ca_xVO_3$ and $Y_{1-x}Ca_xVO_3$ in Fig. 5. In both cases, γ rapidly increases at low doping, indicating the mass enhancement of correlated electrons. The value of γ appears to slightly decrease as x_c is crossed from the metallic side, which is qualitatively consistent with observations in previously studied filling-controlled transitions such as $V_{2-y}O_3$,[33] $LaTiO_{3+\delta/2}$,[34] and $La_{1-x}Sr_xVO_3$.[8] Although we have a rather low density of data points, there is no evidence for a rapid increase in γ on approaching x_c from the metallic side, as often observed for bandwidth-controlled transitions.[1] We note, however, that a divergence in γ at x_c was previously found for $Y_{1-x}Ca_xVO_3$.[15] Our maximum values of γ are comparable to those previously reported for $La_{1-x}Sr_xVO_3$. However, our data differ from those of $La_{1-x}Sr_xVO_3$ in that there is no sharp fall in γ as x_c is crossed toward the insulating side. For $Y_{1-x}Ca_xVO_3$, the downturn in C/T for $x \leqslant 0.4$ at low temperature [Fig. 4(b), inset], shows a deviation from the $C=\gamma T+\beta T^3$ relationship, as expected for an insulator. The large apparent values of γ extrapolated from the linear portion of the plot at higher temperatures may imply that there is a finite density of states close to the Fermi level well into the insulating state, as proposed in the filling-controlled system $LaTiO_{3+\delta/2}$.[34] However, our values of $\sim$25 mJ/mol K^2 for $Y_{0.8}Ca_{0.2}VO_3$ and $\sim$35 mJ/mol K^2 for $Sm_{0.8}Ca_{0.2}VO_3$ are surprisingly high for doping levels relatively far from x_c.

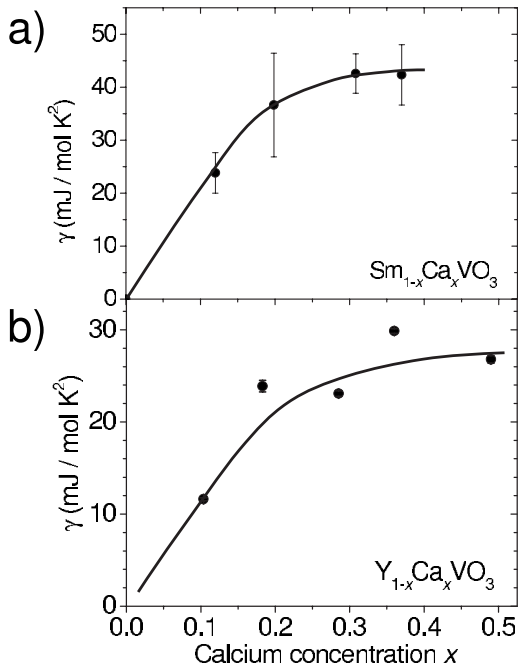

FIG. 5. Evolution of the electronic term of the specific heat, γ, with x for (a) $Sm_{1-x}Ca_xVO_3$ and (b) $Y_{1-x}Ca_xVO_3$. The solid lines are guides for the eye.

II. DISCUSSION

Although the primary effect of Ca doping in the RVO_3 system is to introduce holes and to control the level of band filling, one should not neglect the structural changes that occur with doping. The ionic radius of Ca^{2+} is larger than that of all three R^{3+} cations in the systems studied here, and Ca doping thus leads to an increase in the perovskite tolerance factor which, in turn, increases the bandwidth. However, we do not find any evidence in our transport measurements for bandwidth-controlled phenomena such as a rapid increase of the electronic term γ as x_c is approached from the metallic side.[1] This indicates that the effect of band filling drives the transition in these systems. Fujioka *et al.*[20] presented a phase diagram of the metallic and insulating regimes in doped RVO_3 as a function of doping level and tolerance factor, and our results are in general agreement with this picture.

Different doping regimes with distinct transport properties can be identified, the limits of which we denote by x_1 and x_c.

$x<x_1$. The compounds display thermally activated behavior both in the resistivity and thermopower data. However, the formation of small polarons leads to a lower value of activation energy extracted from the thermopower data than from the resistivity data. The number of charge carriers is small and, at low temperatures, the resistance is too large to measure. The situation can be described using a model where the two Hubbard bands are separated by an energy U. The activation energy corresponds to the thermal excitation of an electron from the lower to the upper Hubbard band.

$x_1<x<x_c$. As the Ca concentration increases, the mechanism of variable-range hopping appears at low temperatures and dominates the thermally activated behavior. This is evident both from the resistivity data, which show a $T^{1/4}$ dependence in the case of $Pr_{1-x}Ca_xVO_3$ and $Y_{1-x}Ca_xVO_3$, and from the thermopower experiments, signaled by a change in sign of the temperature dependence of the Seebeck coefficient. It corresponds to a filling of states in the Hubbard gap, and the band tails start to overlap. However, a metallic behavior is not yet observed, as explained by Anderson and

Mott.[27] Disorder leads to the localization of electrons (Anderson localization). It has been shown by Anderson that the electronic wave function in a random potential may be profoundly altered if the randomness is sufficiently strong.

$x > x_c$. The compounds are metallic, the number of charge carriers has markedly increased, and the transport behavior can be described by Fermi-liquid theory over at least part of the measured temperature range. In the Sm and Y series, a Fermi-liquid behavior is observed over the entire temperature range at doping levels well above x_c, but this is not the case in the Pr series, where the low-temperature resistivity shows an upturn as far as $x=0.6$, which is the highest doped sample in our study. Fermi-liquid theory assumes that a system is homogeneous. However, if it contains defects, then the electrons can be backscattered instead of moving freely. It is known that if a metal contains a high enough concentration of defects, electrons will be weakly localized. Decreasing temperature will then induce a transition from a delocalized to a localized state (Anderson localization). The elastic scattering of electrons from impurities and lattice defects determines the residual resistance of metals at low temperatures. Scattering by random potentials will cause the Bloch waves to lose coherence on the length scale of the mean free path (the distance over which an electron fluctuates by about 2π). In the case of very weak disorder, the wavelength of the electron is smaller than the mean free path and the wave function remains extended throughout the sample. However, in the case of strong disorder, Anderson showed that the wave function will be localized. This theory predicts that in a three-dimensional system, the conductivity will follow a $\sqrt{T}$ dependence, as observed at low temperature at doping levels close to x_c. The anomalous low-temperature resistivity may also be the result of other interactions. It has been shown that in a disordered Fermi liquid, an anomalous behavior occurs close to the Fermi level because of the diffusive character of the electron motion. This also leads to a $\sqrt{T}$ dependence of the resistivity at low temperatures. It is possible that this behavior originates from both weak localization and electron interaction effects. However, experimentally, weak localization is mainly responsible for the anomalous behavior in our materials. We note that in $\mathrm{La}_{1-x}\mathrm{Sr}_x\mathrm{VO}_3$, the resistivity in the lower-doped part of the PM regime has been reported to show a $T^{1.5}$ dependence,[7,8] which was attributed to the effects of strong AF spin fluctuations. We do not observe this behavior, possibly because the AF exchange interactions are weaker in the more distorted perovskite structures of the systems studied here.

Kadowaki and Woods phenomenologically found that the electronic specific heat coefficient scales linearly with the coefficient of the T^2 dependence of the resistivity for compounds in which the electron-electron interactions dominate.[35] For both $\mathrm{Sm}_{1-x}\mathrm{Ca}_x\mathrm{VO}_3$ and $\mathrm{Y}_{1-x}\mathrm{Ca}_x\mathrm{VO}_3$, we find values that are in good agreement with this "universal" behavior. This is evidence that the T^2 dependence of the resistivity originates from electron-electron interactions as described by Fermi-liquid theory.

It is informative to compare the characteristics of the IM transition in hole-doped $R\mathrm{VO}_3$ and $R\mathrm{TiO}_3$. Because V d orbitals are somewhat less extended than Ti d orbitals, one may expect that the one-electron bandwidth W for a given $R\mathrm{VO}_3$ material is narrower than that for the corresponding $R\mathrm{TiO}_3$. Therefore, $R\mathrm{TiO}_3$ materials lie closer to the IM transition than their $R\mathrm{VO}_3$ analogs; for example, the Mott–Hubbard gap is approximately 0.2 eV for LaTiO_3 (Ref. 36) and 1.0 eV for LaVO_3.[14] It follows that in order to reach the IM transition by band filling, a given $R\mathrm{TiO}_3$ material requires fewer doped holes than the corresponding $R\mathrm{VO}_3$ material. This is clear in the case of $\mathrm{La}_{1-x}\mathrm{Sr}_x\mathrm{TiO}_3$, which undergoes the IM transition at $x_c=0.05$,[37] whereas $\mathrm{La}_{1-x}\mathrm{Sr}_x\mathrm{VO}_3$ undergoes the transition at $x_c=0.178$.[8] A further consequence of this difference in W is that the degree of disorder present at the IM transition for a given $R_{1-x}A_x\mathrm{VO}_3$ system (A =divalent cation), due largely to the random potential arising from the distribution of R and A cations, will be greater than that for the corresponding $R_{1-x}A_x\mathrm{TiO}_3$ system. In our measurements, disorder is manifested in the form of variable-range hopping on the insulating side of the transition and in the low-temperature deviation of the resistivity from a T^2 dependence on the metallic side. Although these characteristics are seemingly absent in $\mathrm{La}_{1-x}\mathrm{Sr}_x\mathrm{TiO}_3$,[37] one may expect them to appear in $\mathrm{Y}_{1-x}\mathrm{Ca}_x\mathrm{TiO}_3$, where the IM transition does not occur until $x_c=0.40$.[38] However, measurements in $\mathrm{Y}_{1-x}\mathrm{Ca}_x\mathrm{TiO}_3$ are complicated by the presence of a first-order structural transition accompanied by a rather broad doping region where metallic and insulating phases coexist. It appears that the degree of disorder in $R\mathrm{TiO}_3$ can be strongly enhanced when hole doping is carried out by introducing cation vacancies; for example, variable-range hopping and low-temperature deviation of the resistivity from a T^2 behavior have been clearly observed in $R_{1-x}\mathrm{Ti}_{1-y}\mathrm{O}_3$, even for R =La.[39,40]

An equivalent way of comparing the filling-controlled IM transitions in doped $R\mathrm{VO}_3$ and $R\mathrm{TiO}_3$ is to focus on the electronic correlation strength U/W. Because $U \approx 4$ eV for both titanates and vanadates and changes little with doping,[41] U/W will be larger in $R\mathrm{VO}_3$. A stronger correlation will also serve to delay the onset of itinerant behavior until higher doping levels, which increases the degree of disorder at the IM transition further. A strong correlation is manifested by high values of the electronic specific heat term γ, both in the metallic and insulating phases, and of $a_{e\text{-}e}$, the coefficient of the T^2 resistivity term in Eq. (4). Our results are consistent with this picture; although the absolute values of γ reported in the literature for doped $R\mathrm{VO}_3$ and $R\mathrm{TiO}_3$ materials vary widely with no obvious systematic trend, our values of up to 40 $\mathrm{mJ/mol\,K^2}$ over a broad doping range are undoubtedly large. A better comparison of the correlation strength in different materials can perhaps be gained from values of $a_{e\text{-}e}$. We observe values of up to 4×10^{-8} $\Omega\,\mathrm{cm/K^2}$ on the metallic side of the transition, an order of magnitude more than the value of 2.5×10^{-9} $\Omega\,\mathrm{cm/K^2}$ reported for $\mathrm{La}_{1-x}\mathrm{Sr}_x\mathrm{TiO}_3$,[37] much greater than the value of 7×10^{-9} $\Omega\,\mathrm{cm/K^2}$ for $\mathrm{Y}_{1-x}\mathrm{Ca}_x\mathrm{TiO}_3$,[38] but equivalent to the value of 3×10^{-8} $\Omega\,\mathrm{cm/K^2}$ for $\mathrm{Nd}_{1-x}\mathrm{TiO}_3$.[40]

CONCLUSION

We have deduced the nature of the IM transition in $R_{1-x}\mathrm{Ca}_x\mathrm{VO}_3$ (R=Pr, Sm, and Y) from electron transport

measurements. With increasing doping, all three series of materials undergo an IM transition induced by band-filling control. Disorder plays an important role in the transition, which takes place via a weakly localized intermediate state before the metallic state is reached by further doping. Strong electron correlations are an important feature of both the insulating and metallic areas of the phase diagram.

ACKNOWLEDGMENTS

We are grateful to G. J. Nieuwenhuys for performing the specific heat measurements and to M. Donker for experimental contributions. We acknowledge financial support by the Netherlands Organisation for Scientific Research (NWO) and the European Project SCOOTMO RTN (Contract No. HPRN-CT-2002-00293).

*Corresponding author. t.t.m.palstra@rug.nl

[1] M. Imada, A. Fujimori, and Y. Tokura, Rev. Mod. Phys. **70**, 1039 (1998).
[2] J. Zaanen, G. A. Sawatzky, and J. W. Allen, Phys. Rev. Lett. **55**, 418 (1985).
[3] M. Sayer, R. Chen, R. Fletcher, and A. Mansingh, J. Phys. C **8**, 2059 (1975).
[4] P. Dougier and P. Hagenmuller, J. Solid State Chem. **15**, 158 (1975).
[5] E. Prasad, M. Sayer, and J. P. Noad, Phys. Rev. B **19**, 5144 (1979).
[6] A. V. Mahajan, D. C. Johnston, D. R. Torgeson, and F. Borsa, Phys. Rev. B **46**, 10973 (1992).
[7] F. Inaba, T. Arima, T. Ishikawa, T. Katsufuji, and Y. Tokura, Phys. Rev. B **52**, R2221 (1995).
[8] S. Miyasaka, T. Okuda, and Y. Tokura, Phys. Rev. Lett. **85**, 5388 (2000).
[9] J. Fujioka, S. Miyasaka, and Y. Tokura, Phys. Rev. Lett. **97**, 196401 (2006).
[10] N. F. Mott, M. Pepper, S. Pollitt, R. H. Wallis, and C. J. Adkins, Proc. R. Soc. London, Ser. A **345**, 169 (1975).
[11] P. Dougier, D. Deglane, and P. Hagenmuller, J. Solid State Chem. **19**, 135 (1976).
[12] H. C. Nguyen and J. B. Goodenough, Phys. Rev. B **52**, 8776 (1995).
[13] K. Maiti, N. Y. Vasanthacharya, and D. D. Sarma, J. Phys.: Condens. Matter **9**, 7507 (1997).
[14] K. Maiti and D. D. Sarma, Phys. Rev. B **61**, 2525 (2000).
[15] K. Kumagai, K. Kawano, T. Suzuki, H. Takahashi, M. Kasuya, Y. Fujishima, Y. Taguchi, Y. Okada, and Y. Tokura, Physica B **186-188**, 1030 (1993).
[16] M. Kasuya, Y. Tokura, T. Arima, H. Eisaki, and S. Uchida, Phys. Rev. B **47**, 6197 (1993).
[17] Y. Nishihara, H. Kawanaka, and H. Bando, Pramana **58**, 737 (2002).
[18] H. Kawanaka, H. Bando, K. Mitsugi, and Y. Nishihara, J. Phys. Soc. Jpn. **71**, 163 (2002).
[19] F. Cintolesi, P. Ghigna, A. Lascialfari, and G. B. Parravicini, Phys. Chem. Chem. Phys. **5**, 4691 (2003).
[20] J. Fujioka, S. Miyasaka, and Y. Tokura, Phys. Rev. B **72**, 024460 (2005).
[21] F. Cintolesi, M. Corti, A. Rigamonti, G. Rossetti, P. Ghigna, and A. Lascialfari, J. Appl. Phys. **79**, 6624 (1996).
[22] H. Nakotte, A. M. Alsmadi, H. Kawanaka, K. Kindo, and K. Goto, Int. J. Mod. Phys. B **16**, 3058 (2002).
[23] F. Wang, J. Zhang, P. Yuan, Q. Yan, and P. Zhang, J. Phys.: Condens. Matter **12**, 3037 (2000).
[24] M. H. Sage, G. R. Blake, G. J. Nieuwenhuys, and T. T. M. Palstra, Phys. Rev. Lett. **96**, 036401 (2006).
[25] G. R. Blake, T. T. M. Palstra, Y. Ren, A. A. Nugroho, and A. A. Menovsky, Phys. Rev. Lett. **87**, 245501 (2001).
[26] M. H. Sage, Ph.D. thesis, University of Groningen, 2006 (http://dissertations.ub.rug.nl/faculties/science/2006/m.h.sage/).
[27] N. F. Mott, *Metal-Insulator Transitions* (Taylor and Francis, London, 1990).
[28] J. M. D. Coey, Philos. Trans. R. Soc. London, Ser. A **356**, 1519 (1998).
[29] Y. Sun, X. Xu, and Y. Zhang, J. Phys.: Condens. Matter **12**, 10475 (2000).
[30] W.-H. Jung, Physica B **304**, 75 (2001).
[31] S. Sen and A. Ghosh, J. Appl. Phys. **86**, 2078 (1999).
[32] I. M. Sutjahja, Ph.D. thesis, University of Amsterdam, 2003.
[33] S. A. Carter, T. F. Rosenbaum, P. Metcalf, J. M. Honig, and J. Spalek, Phys. Rev. B **48**, 16841 (1993).
[34] Y. Taguchi, T. Okuda, M. Ohashi, C. Murayama, N. Mori, Y. Iye, and Y. Tokura, Phys. Rev. B **59**, 7917 (1999).
[35] K. Kadowaki and S. B. Woods, Solid State Commun. **58**, 507 (1986).
[36] Y. Okimoto, T. Katsufuji, Y. Okada, T. Arima, and Y. Tokura, Phys. Rev. B **51**, 9581 (1995).
[37] Y. Tokura, Y. Taguchi, Y. Okada, Y. Fujishima, T. Arima, K. Kumagai, and Y. Iye, Phys. Rev. Lett. **70**, 2126 (1993).
[38] M. Tsubota, F. Iga, T. Nakano, K. Uchihira, S. Kura, M. Takemura, Y. Bando, K. Umeo, T. Takabatake, E. Nishibori, M. Takata, M. Sakata, K. Kato, and Y. Ohishi, J. Phys. Soc. Jpn. **72**, 3182 (2003).
[39] H. D. Zhou and J. B. Goodenough, Phys. Rev. B **71**, 165119 (2005).
[40] A. S. Sefat, J. E. Greedan, G. M. Luke, M. Niéwczas, J. D. Garrett, H. Dabkowska, and A. Dabkowski, Phys. Rev. B **74**, 104419 (2006).
[41] A. E. Bocquet, T. Mizokawa, K. Morikawa, A. Fujimori, S. R. Barman, K. Maiti, D. D. Sarma, Y. Tokura, and M. Onoda, Phys. Rev. B **53**, 1161 (1996).